

Multistability and nonsmooth bifurcations in the quasiperiodically forced circle map

HINKE OSINGA

School of Mathematical Sciences,
University of Exeter, Exeter EX4 4QE, UK

h.m.osinga@exeter.ac.uk

JAN WIERSIG

Max-Planck-Institut für Physik komplexer Systeme,
D-01187 Dresden, Germany

jwiersig@mpipks-dresden.mpg.de

PAUL GLENDINNING

Department of Mathematics,
UMIST, Manchester M60 1QD, UK

p.a.glendinning@umist.ac.uk

ULRIKE FEUDEL

Institut für Physik,
Universität Potsdam, PF 601553, D-14415 Potsdam, Germany

ulrike@agnld.uni-potsdam.de

October 25, 2018

Abstract

It is well-known that the dynamics of the Arnol'd circle map is phase-locked in regions of the parameter space called Arnol'd tongues. If the map is invertible, the only possible dynamics is either quasiperiodic motion, or phase-locked behavior with a unique attracting periodic orbit. Under the influence of quasiperiodic forcing the dynamics of the map changes dramatically. Inside the Arnol'd tongues open regions of multistability exist, and the parameter dependency of the dynamics becomes rather complex. This paper discusses the bifurcation structure inside the Arnol'd tongue with zero rotation number and includes a study of nonsmooth bifurcations that happen for large nonlinearity in the region with strange nonchaotic attractors.

1 Introduction

The Arnol'd circle map [Arnol'd, 1965]

$$x_{n+1} = x_n + \Omega + \frac{K}{2\pi} \sin(2\pi x_n) \pmod{1} \quad (1)$$

is one of the paradigms for studying properties of nonlinear dynamical systems, both because it is a very simple map, and because of its great physical relevance (see, e.g. [Bohr et al., 1985]). Using the circle map one can model the structure of phase-lockings (devil's staircase) of a periodically forced nonlinear oscillator [Jensen et al., 1983; Jensen et al., 1984] and the current-voltage characteristics of a driven Josephson junction [Bohr et al., 1984]. The phase-locked regions of the Arnol'd circle map form the well-known Arnol'd tongues [Arnol'd, 1983; Hall, 1984]. If $|K| < 1$ there is a unique periodic attractor with a particular rotation number in each tongue.

In this paper we study the structure of the phase-locked regions of the Arnol'd circle map driven by a rigid rotation with an irrational frequency. This system exhibits different kinds of dynamics, namely quasiperiodic motions with two and three incommensurate frequencies, chaotic attractors, and strange nonchaotic attractors (SNAs). SNAs have a strange geometrical structure, but unlike chaotic attractors they do not exhibit a sensitive dependence to changes in the initial conditions, i.e. their dynamics is not chaotic. They have been found in many quasiperiodically forced systems [Grebogi et al., 1984], and also in the quasiperiodically forced circle map [Ding et al., 1989; Feudel et al., 1995].

Previous investigations show that regions of bistability occur in phase-locked regions of the quasiperiodically forced circle map [Glendinning et al., 2000] and the phase-locked regions change in shape depending on the strength of the forcing. This change in shape is related to the emergence of SNAs [Feudel et al., 1997]. Based on these studies the aim of this paper is twofold. We study regions in parameter space where more than two attractors coexist (pockets of multistability). Secondly, we discuss the relation between these multistable regions and the appearance of strange nonchaotic attractors. In our discussion of the way these attractors are created and destroyed we are led to a description of nonstandard (nonsmooth) bifurcations of the invariant curves.

If the unforced circle map is modified by introducing additional nonlinearities, coexisting attractors with the same rotation number can occur within the phase-locked regions [McGehee & Peckham, 1996]. In our system, multistability within the phase-locked regions is induced by the forcing rather than an additional nonlinear term. In quasiperiodically forced systems the coexisting attractors may be either invariant curves or SNAs depending on the strength of the forcing. Our investigation focuses on how these multistable regions appear and disappear under variation of the system's parameters: the nonlinearity K and the forcing amplitude ε . For the tongue with zero rotation number the multistable regions open and close by *smooth* saddle-node or pitchfork bifurcations of invariant curves if K and ε are small. For larger K these saddle-node and pitchfork bifurcations become *nonsmooth*: instead of merging uniformly (smooth bifurcation), the relevant stable and unstable invariant curves appear to collide only in a dense set of points.

The paper is organized as follows. Section 2 recalls important properties of the Arnol'd circle map relevant for this study and their changes under the influence of quasiperiodic forcing. In particular we discuss the phase-locked region with zero rotation number. Within this phase-locked region we find pockets of multistability with a rather complex bifurcation structure which is analyzed in Sec. 3. Smooth and nonsmooth saddle-node and pitchfork bifurcations, leading to coexisting attractors, are studied in Sec. 4 to get a better understanding of the changes in the bifurcation structure depending on the strength of nonlinearity and forcing. Furthermore, we

investigate the transition between smooth and nonsmooth bifurcations and its implications to the dynamics of the system. In the full parameter space we find bifurcations of codimension two. In Sec. 5 we discuss a special codimension-2 point that involves only nonsmooth bifurcations. It turns out that the unfolding of this point is very different from the smooth analog. Finally, in Sec. 6, we briefly discuss phase-locked regions with small, but finite, rotation number. We conclude this paper with a summary in Sec. 7 and an Appendix with details on the numerical computations. For readers with a black and white copy of this article we provide a supplementary website [Osinga et al., 2000].

2 The Quasiperiodically Forced Circle Map

The quasiperiodically forced circle map is a map on the torus with lift

$$x_{n+1} = x_n + \Omega + \frac{K}{2\pi} \sin(2\pi x_n) + \varepsilon \sin(2\pi \vartheta_n), \quad (2)$$

$$\vartheta_{n+1} = \vartheta_n + \omega \pmod{1}, \quad (3)$$

where ϑ_n and x_n modulo 1 give the coordinates on the torus. The parameter Ω is the phase shift, K denotes the strength of nonlinearity ($K > 0$), ε is the forcing amplitude, and the forcing frequency ω is irrational. Throughout this paper we choose to work with $\omega = (\sqrt{5} - 1)/2$.

2.1 The unforced system

Let us recall the behavior of the unforced circle map (1). The dynamics of this map can be either periodic, quasiperiodic, or chaotic, depending on the parameters Ω and K . The critical line $K = 1$ divides the parameter space into two regions. If $K < 1$ the map is invertible and the motion can only be periodic (phase-locked) or quasiperiodic. For $K > 1$ the map is noninvertible and chaotic motion is possible.

The rotation number is used to characterize the different kinds of motion. It is defined as

$$\rho(\Omega, K) = \lim_{N \rightarrow \infty} \frac{x_N - x_0}{N}, \quad (4)$$

where x_N is the N th iterate of (1), starting from x_0 . It can be shown that $\rho(\Omega, K)$ does not depend on x_0 if $K < 1$. If the rotation number is rational, the attracting motion is periodic, otherwise it is quasiperiodic. For $K < 1$ the parameter space is split into regions with rational rotation number, the phase-locked regions or Arnol'd tongues, and regions with irrational rotation number corresponding to quasiperiodic motion. For example, the main tongue, the phase-locked region with zero rotation number, is bounded by the curves $\Omega = \pm\Omega_0(K)$, where $\Omega_0(K) = K/2\pi$. For any choice of Ω and K , with $|\Omega| < \Omega_0$ and $K < 1$, there are exactly two fixed points, one is attracting and the other is repelling. At the boundary $|\Omega| = \Omega_0$ the two fixed points are annihilated in a saddle-node bifurcation. For other rotation numbers $\rho \neq 0$ the K -dependency of the boundary $\Omega_\rho(K)$ is nonlinear, but it is always a curve of saddle-node bifurcations.

2.2 The forced system

A variety of behavior is possible in the coupled maps (2)–(3). The rotation number (4) exists, but depends on ε and ω in addition to Ω and K , and the direct analogs of the periodic and quasiperiodic motion of the uncoupled Arnol'd map are invariant curves (the graph of a function $\vartheta \mapsto x(\vartheta)$) and motion which is dense on the torus, respectively. In the former case the rotation number is rationally related to ω ($\rho = r_1 + r_2\omega$ with r_i rational, $i = 1, 2$) and in the latter

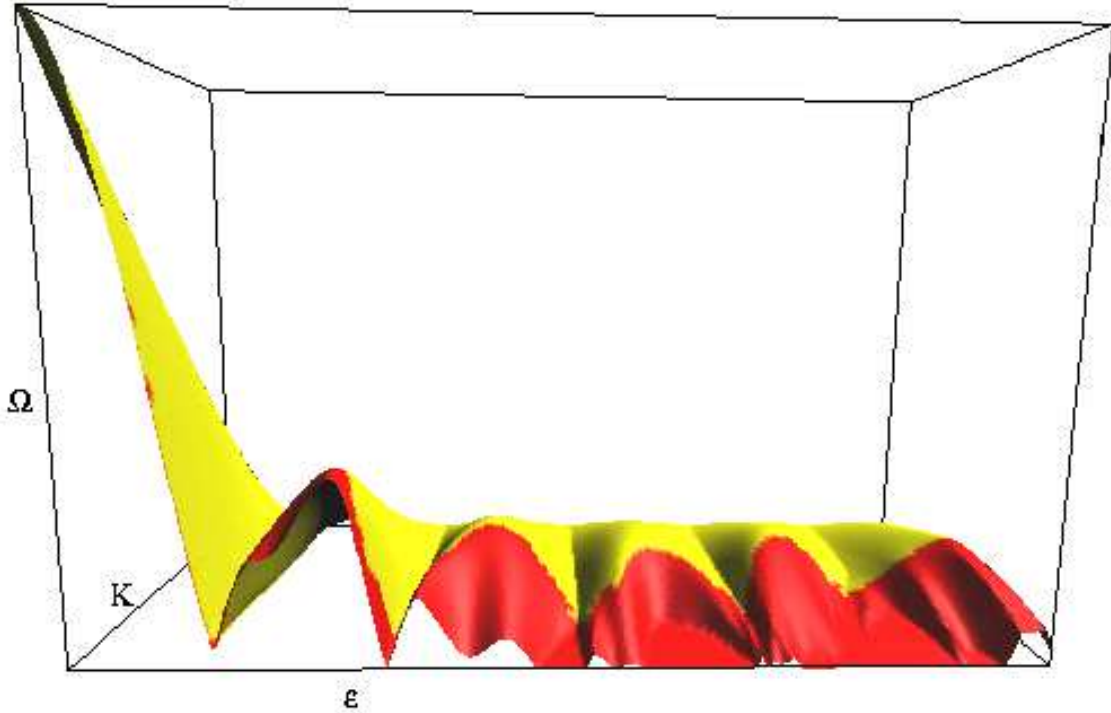


Figure 1: The boundary $|\Omega| = \Omega_0(\varepsilon, K)$ of the phase-locked region with zero rotation number; $\varepsilon \in [0, 5]$ runs from left to right, $K \in [0, 1]$ from back to front, and $|\Omega| \in [0, 0.16]$ from bottom to top. Pairs of invariant curves inside the phase-locked region ($|\Omega| < \Omega_0$) are annihilated at its boundary leading either to three-frequency quasiperiodic motion (yellow area) or SNAs (red area); see App. A.1.

case there is no such rational relation. For both rationally and irrationally related rotation numbers strange nonchaotic attractors (SNAs) may also be possible. An SNA has a strange geometric structure, that is, it can be viewed as the graph of an everywhere discontinuous function $\vartheta \mapsto x(\vartheta)$, but the dynamics on the attractor is not chaotic, because typical Lyapunov exponents in the x -direction are negative (there is always a zero Lyapunov exponent in the ϑ -direction).

If the rotation number is rationally related to ω then the motion is said to be *phase-locked* and the regions of parameter space in which the motion is phase-locked are analogous to the Arnol'd tongues of the unforced map. On the boundaries of the phase-locked regions we expect to see saddle-node bifurcations. There is an additional complication in the forced maps [Feudel et al., 1995] in that the saddle-node bifurcations may be smooth (two invariant curves converge uniformly from inside the phase-locked region) or nonsmooth. In the smooth saddle-node bifurcation the nontrivial Lyapunov exponent in the x -direction goes to zero at the bifurcation point. In the nonsmooth saddle-node bifurcation the two invariant curves appear to collide only on a dense set of points. Moreover, the typical nontrivial Lyapunov exponent remains negative. These nonsmooth saddle-node bifurcations seem to be associated with the appearance of SNAs outside the phase-locked region [Ding et al., 1989; Feudel et al., 1995; Glendinning, 1998].

It can be shown that one mechanism of the appearance of SNAs is related to changes in the shape of the phase-locked regions [Feudel et al., 1997; Glendinning et al., 2000]. For the unforced map the width of a phase-locked region increases monotonically with increasing nonlinearity K ; this is no longer the case for positive forcing amplitude ε . Moreover, as Fig. 1 shows, for fixed K the width of the phase-locked region oscillates as ε increases. In particular, there are certain values of ε for which the width of the phase-locked region becomes extremely small.

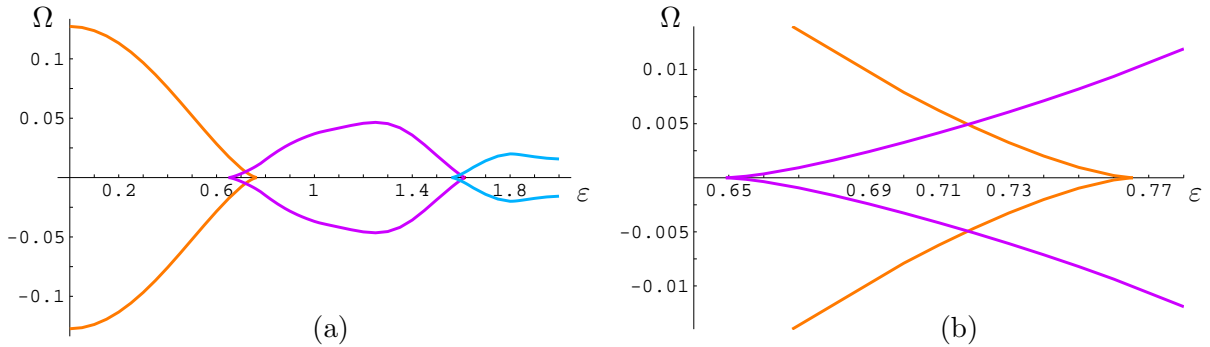


Figure 2: The bifurcation structure for $K = 0.8$ of the phase-locked region with zero rotation number (a) with detail of the first overlap (b).

Unfortunately, using only numerical methods, we cannot decide whether the region actually closes or not at those ε -values. For more details on numerical computations we refer to App. A.1.

For small fixed nonlinearity K the boundary $\Omega_0(\varepsilon, K)$ of the phase-locked region can be approximated by (the modulus of) a Bessel function of order zero using first order perturbation theory [Glendinning et al., 2000]. Numerical simulations also revealed regions of bistability in the vicinity of the zeroes of the Bessel function, where the width of the phase-locked region is very small. The bistability regions are bounded by saddle-node bifurcations of invariant curves, which has been confirmed by second order perturbation theory [Glendinning & Wiersig, 1999].

The study in [Glendinning et al., 2000; Glendinning & Wiersig, 1999] only applies for K close to 0. We wish to study what happens to the phase-locked region with zero rotation number for larger K . However, we restrict our considerations to the invertible case $K < 1$, so that chaos is ruled out. We find that the regions of bistability contain other regions where even more attractors coexist. In the following we describe how these regions appear and disappear as a parameter varies. We also study smooth and nonsmooth bifurcations and make some remarks on the appearance of SNAs.

The majority of the rest of this paper describes the results of numerical simulations of Eqs. (2)–(3). As such, the reader should bear in mind that our conclusions are based on numerical observations and may turn out to be misleading in places. We have made every effort to avoid such problems (see the Appendix) and believe that the phenomena reported are sufficiently interesting and mathematically intractable to merit this numerical investigation, even if we remain uncertain of some of the outcomes. The reader is encouraged to maintain a healthy scepticism throughout.

3 The Internal Structure of the Main Tongue for $K = 0.8$

In the simplest case the boundary $|\Omega| = \Omega_0(\varepsilon, K)$ represents the disappearance of two invariant curves, a stable and an unstable one. However, for $|\Omega| < \Omega_0(\varepsilon, K)$ more than two invariant curves may exist that disappear before this boundary is crossed. Such pockets of multistability are found near local minima of $\Omega_0(\varepsilon, K)$, cf. the region of bistability predicted by perturbation analysis for small K [Glendinning et al., 2000; Glendinning & Wiersig, 1999]. For example, Fig. 2(a) shows a cross-section of Fig. 1 at $K = 0.8$, with both positive and negative sides of the boundary of the phase-locked region. The outer boundary is the function $|\Omega| = \Omega_0(\varepsilon, 0.8)$. Extra curves are drawn marking the boundaries of pockets of multistability, which is best seen in the enlargements Figs. 2(b), 4 and 5. These pockets of multistability can be considered as overlaps of different “bubbles” with the same rotation number as in Fig. 2(a). For better visualization

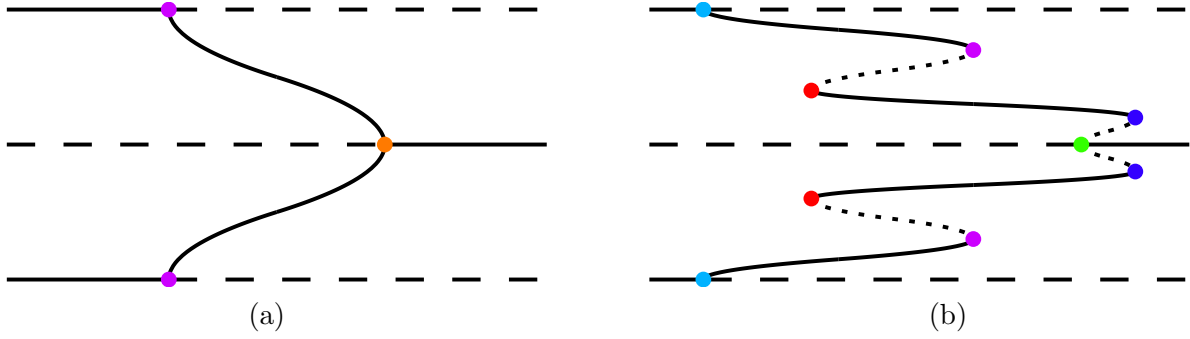


Figure 3: Sketch of the bifurcations along the line $\Omega = 0$ and $K = 0.8$ in the first (a) and second (b) overlap. Shown are invariant circles (represented by one point) versus ε . Closed curves represent stable and dashed curves represent unstable circles. The colors correspond with the colors of the bifurcation curves in Figs. 2, 4 and 5.

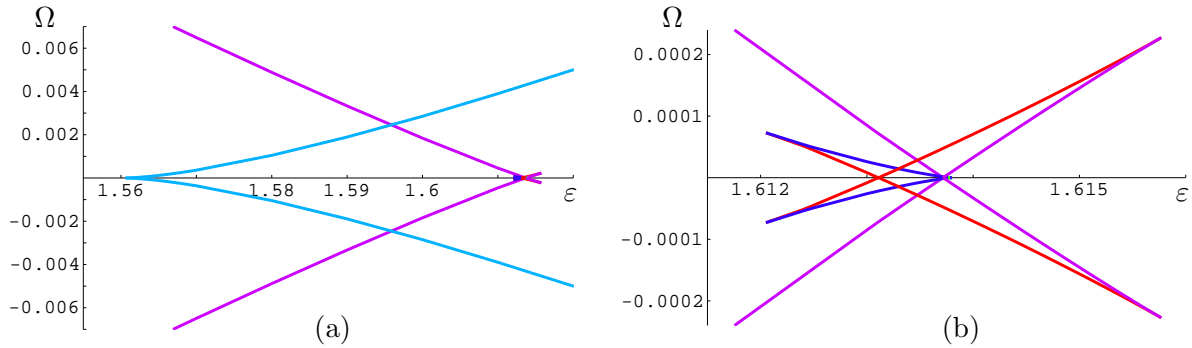


Figure 4: The bifurcation structure for $K = 0.8$ in the second overlap (a) seems to be the same as in Fig. 2(b). However, an enlargement (b) shows that the structure is much more complicated.

we have chosen different colors for bifurcations of different pairs of invariant curves.

3.1 Bifurcations for $K = 0.8$ in the first region of overlap

The first overlap is enlarged in Fig. 2(b). The orange and purple curves enclose a rhombus shaped region where two attracting and two repelling invariant circles exist. This region of bistability is bounded by curves of saddle-node bifurcations that end in pitchfork bifurcations on the line $\Omega = 0$. Note that if $\Omega = 0$ the map has a symmetry ($x \mapsto -x$, $\vartheta \mapsto \vartheta + 1/2$) which implies that the rotation number in the x -direction is always zero and pitchfork bifurcations should be expected. The bifurcation sequence for $\Omega = 0$ is sketched in Fig. 3(a) where each circle is represented as a point and ε increases along the horizontal axis. The bottom and top lines are identical, representing the modulo 1 computations. The purple and orange dots are the pitchfork bifurcations that mark the crossing of the purple and orange curves in Fig. 2(b) along $\Omega = 0$, respectively.

3.2 Bifurcations for $K = 0.8$ in the second region of overlap

Figure 4(a) shows a detail of the second overlap. This picture is very similar to Fig. 2(b), but the bifurcation diagram along $\Omega = 0$ in Fig. 3(b) reveals a more complex structure. Let us first discuss Fig. 3(b). The first bifurcation (light blue dot) is the same pitchfork bifurcation as the purple dot in Fig. 3(a): the stable circle becomes unstable, creating two new stable circles. As ε increases two other stable circles are born in a pair of saddle-node bifurcations (red dots). We

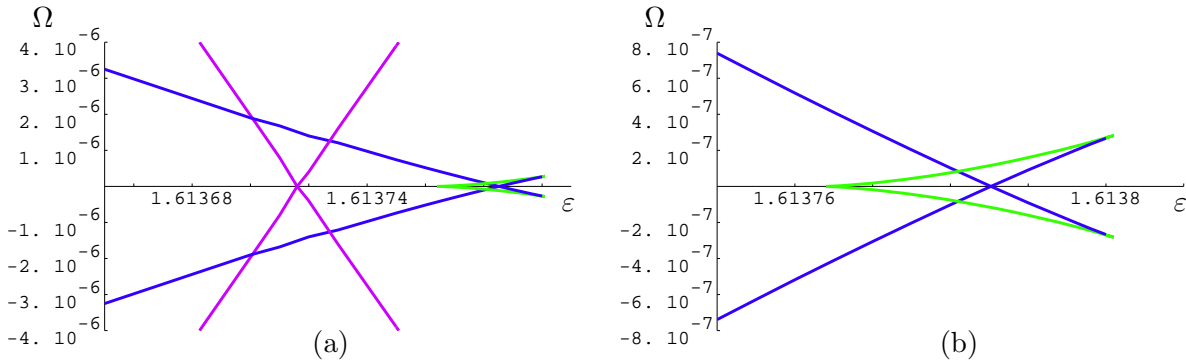


Figure 5: Details of the bifurcation structure for $K = 0.8$ in the second overlap. The last pitchfork bifurcation on the line $\Omega = 0$ is subcritical (b) as opposed to supercritical in Fig. 2(b).

now have four different attractors. Note that these saddle-node bifurcations happen at the same values of ε due to the symmetry along the line $\Omega = 0$, as referred to earlier.

At the purple dots the two attracting circles from the pitchfork bifurcation disappear in a pair of saddle-node bifurcations. Note that this pair of saddle-node bifurcations is connected to the purple pitchfork bifurcation of Fig. 3(a) via the purple curve off $\Omega = 0$ in Fig. 2(a). We are now left with two attractors and two repellers. These last two attractors do not disappear in a pitchfork bifurcation as in Fig. 3(a) (orange dot). Instead, they disappear in a pair of saddle-node bifurcations (dark blue dots) with two repellers that are born in a pitchfork bifurcation (green dot) for slightly smaller ε . Note that this pitchfork bifurcation is subcritical, as opposed to the supercritical orange one in Fig. 3(a).

The unfolding of these bifurcations inside the phase-locked region with $\Omega \neq 0$ is shown in detail in Figs. 4 and 5. The curves are colored according to the colors of the bifurcations in Fig. 3(b). As expected, for $\Omega \neq 0$ pairs of saddle-node bifurcations no longer happen at the same values of ε . They form two different curves that cross each other exactly at $\Omega = 0$. We already mentioned earlier that the purple curves connect all the way left in a pitchfork bifurcation on the line $\Omega = 0$ in the first overlap. The light blue curves start in the pitchfork bifurcation at $\Omega = 0$ and become the outer boundary $|\Omega| = \Omega_0(\varepsilon, 0.8)$ once they cross the purple curves. The red curves form swallowtails with the purple curves on the right side and the dark blue curves on the left side; see Fig. 4(b). Finally, the dark blue curves form swallowtails with red and green curves; see Fig. 5.

4 The Structure of Bifurcations in the (ε, K) -plane

The bifurcation structure depends on the strength of the nonlinearity K . We study the two-parameter dependence only on the cross-section $\Omega = 0$, because the unfolding inside the phase-locked region with $\Omega \neq 0$ is similar to that discussed in Sec. 3. As expected, the regions of overlap change shape with K . In particular, only the regions with no more than two attractors persist for small K and moderate ε . This is shown in Fig. 6 with a cross-section at $\Omega = 0$ in the (ε, K) -plane of the second overlap; see App. A.2 for details on how this picture was generated.

In the following sections we describe the bifurcations in more detail. Section 4.1 discusses the sequence of bifurcations that happen as K decreases. For small K (less than approximately 0.8 for the bifurcations we have looked at), saddle-node and pitchfork bifurcations happen via a uniform collision of invariant curves: at the moment of bifurcation, two (saddle-node) or three (pitchfork) curves merge at *each* value of ϑ . We call these bifurcations *smooth* bifurcations. For K close to 1 the attractors may become extremely wrinkled, which gives rise to *nonsmooth*

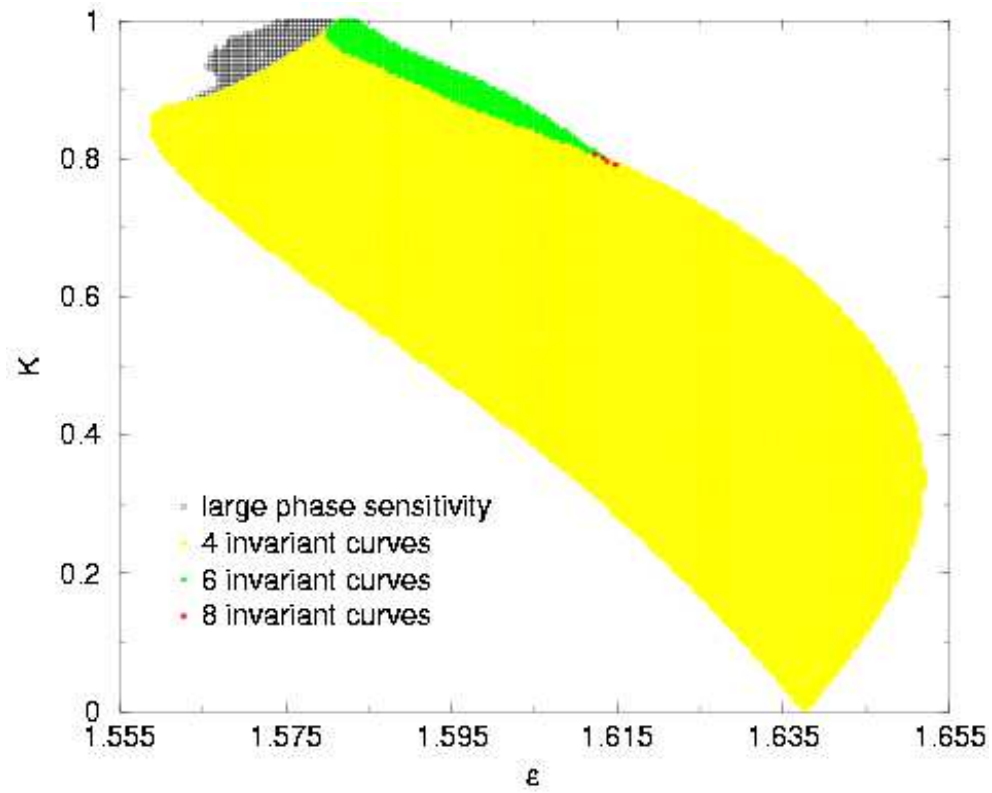


Figure 6: A cross-section at $\Omega = 0$ of the second overlap over a 200×200 grid. A point in the white region corresponds to two invariant curves, one is stable and the other is unstable. The region in which the stable curve is extremely wrinkled (large phase sensitivity, see App. A.2) is marked as well.

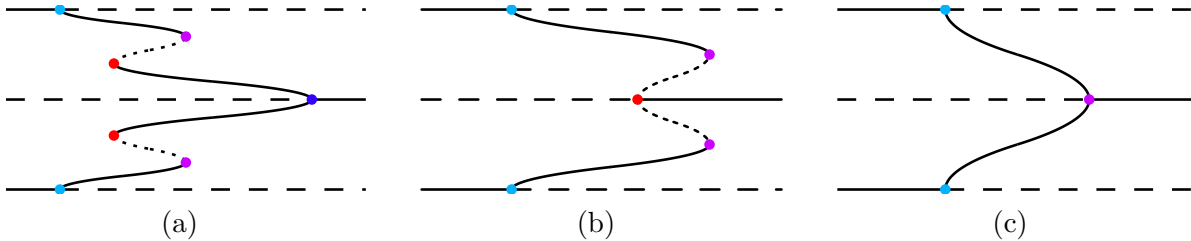


Figure 7: Sketches of the bifurcations along the line $\Omega = 0$ in the second overlapping region as K decreases from 0.8 to 0. The bifurcation structure of Fig. 3(b) for $K = 0.8$ transforms into one like Fig. 3(a) by “absorbing” pairs of saddle-node bifurcations in the second pitchfork bifurcation.

bifurcations: at the moment of bifurcation the invariant curves now collide only in a dense set of ϑ -values. The nonsmooth pitchfork and nonsmooth saddle-node bifurcations are described in detail in Secs. 4.2 and 4.3, respectively.

4.1 Smooth bifurcations for $\Omega = 0$ in the second region of overlap

Figure 6 indicates that at most two attractors exist for small K and moderate ε . This means that for fixed small K , the bifurcation portrait looks like Fig. 3(a). Hence, as we decrease K from $K = 0.8$ to 0, the extra pairs of saddle-node bifurcations (see Fig. 3(b)) need to disappear somehow. It turns out that the last pitchfork bifurcation, the green dot in Fig. 3(b), “absorbs” these saddle-node bifurcations one by one. In doing so, the pitchfork bifurcation switches from subcritical to supercritical and vice versa (a standard codimension-2 bifurcation). A sketch of this process along the line $\Omega = 0$ is shown in Fig. 7(a)–(c).

In the (Ω, ε) -plane the picture changes as follows. The first swap, Fig. 7(a), comes about as the pitchfork point and the intersection point of the dark blue curves on $\Omega = 0$ collapse; see Fig. 5(b). When K decreases, these points move closer together, causing the slope of the dark blue curves to become steeper and the ends of the swallowtail to move closer to $\Omega = 0$. Upon collision the green curves disappear and the dark blue curves end in a supercritical pitchfork bifurcation.

In the second swap the dark blue curves disappear in a similar way via a collision of the pitchfork point and the intersection point of the two red curves, making the pitchfork subcritical again. Note that, in order for this to happen, the pitchfork point crosses the intersection point of the two purple curves; compare Figs. 4(b) and 5(a). Figures 7(a)–(b) show why this is a crossing and not a collision: the pair of purple saddle-node bifurcations happens “far out” in state space from the pitchfork bifurcation. Therefore, the crossing is only a crossing in this projection on the (Ω, ε) -plane.

The third swap, Fig. 7(c), is identical to the first, causing the disappearance of the red curves. In this bifurcation diagram at most two attractors coexist, which is the desired situation for K small.

4.2 Nonsmooth pitchfork bifurcations

For K close to 1 the situation is more complicated, because some of the invariant curves are very wrinkled and the pitchfork bifurcation becomes nonsmooth. This bifurcation has been found by Sturman [1999] in a similar map. Let us discuss what happens for $\Omega = 0$, along the line $K = 0.9$ as we approach the pitchfork bifurcation by decreasing ε , starting in the yellow region in Fig. 6. Figure 8(a) shows all invariant curves just before the bifurcation. The two stable invariant curves (black and blue) correspond to the two outer branches of the pitchfork, the unstable invariant curve (red) relates to the inner branch of the pitchfork separating the two outer ones.

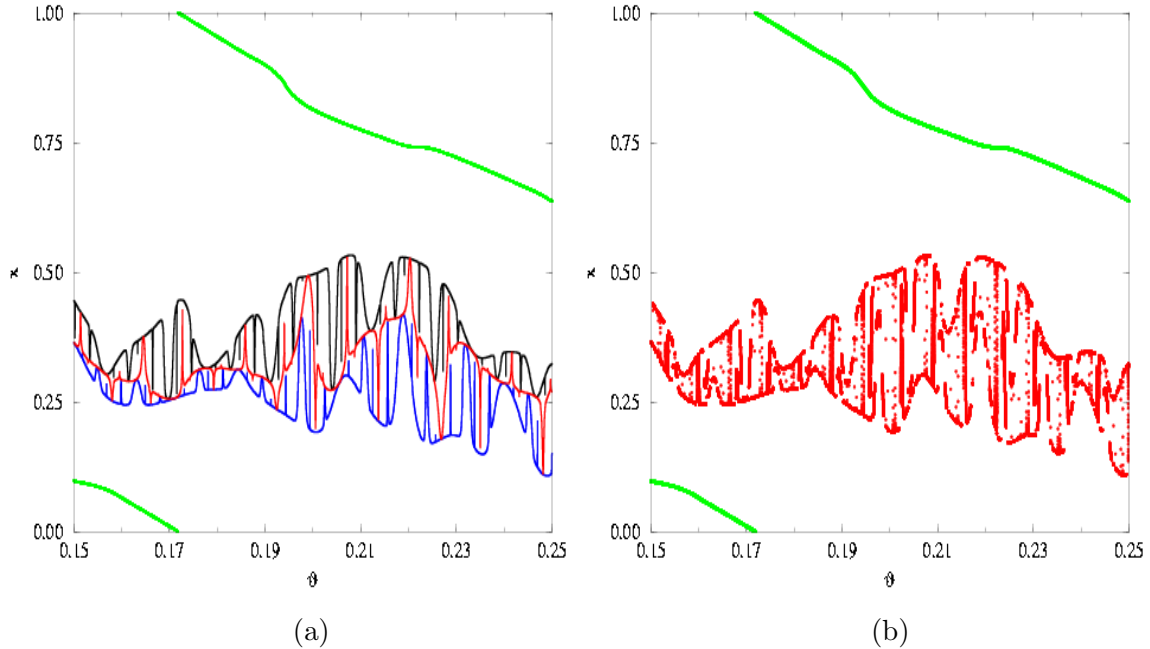


Figure 8: Nonsmooth pitchfork bifurcation with $\Omega = 0$ and $K = 0.9$: (a) before the collision ($\varepsilon = 1.56765$): attractors in blue and black, unstable invariant curves in green and red; (b) after the collision ($\varepsilon = 1.5675$): SNA (red) and the unstable invariant curve not taking part in the bifurcation (green).

The fourth invariant curve (green) is also unstable, but it is “far away” and does not take part in the bifurcation. As we decrease ε towards the bifurcation point the three invariant curves (blue, black and red) approach each other, but due to their wrinkled structures they appear to collide only in a dense set of ϑ -values instead of merging uniformly as in a smooth bifurcation. This indicates that at the moment of bifurcation the attractor is an SNA. Numerical evidence suggests that this SNA persists and smoothes out to an invariant curve over a small ε -interval; see for example the red attractor in Fig. 8(b) for ε below the bifurcation value. It is possible that we see the reverse of *fractalization*, a mechanism for the appearance of SNAs reported in [Nishikawa & Kaneko, 1996]. However, if we use the method of rational approximations for testing whether the attractor is an SNA, we get conflicting results; see App. A.3 for more details. We remark that we get these conflicting numerical results only for the nonsmooth pitchfork bifurcation. In any case, after a further decrease in ε the attractor is clearly a smooth invariant curve.

It is important to note that the nonsmooth pitchfork bifurcation is uniquely defined as the moment of collision of three invariant curves and the locus of bifurcation lies on a curve in the (ε, K) -plane. The process of fractalization is a gradual process where the moment of transition from an invariant curve to an SNA is not well-defined numerically. We wish to emphasize that it is, therefore, completely unclear whether the set of parameter pairs (ε, K) with $\Omega = 0$ that exhibit SNAs after the nonsmooth pitchfork bifurcation has zero or finite size.

Since the boundary of the region of bi- or multistability for $\Omega = 0$ is given by smooth and nonsmooth pitchfork bifurcations there is a codimension-2 point in the (ε, K) -plane where the smooth and the nonsmooth pitchfork bifurcation curves meet. An approximation of this codimension-2 point is $(\varepsilon, K) = (1.564, 0.89)$. In any neighborhood of this point we always find all three kinds of dynamical behaviors: one stable invariant curve, two stable invariant curves, and one SNA; although the latter may only exist on the nonsmooth bifurcation curve itself.

4.3 Nonsmooth saddle-node bifurcations

If K is small and ε moderate then the saddle-node bifurcations observed numerically involve two invariant curves on the torus which converge and destroy each other. At larger values of K , simulations suggest that two invariant curves touch on an orbit at the bifurcation point, so points of intersection of these sets are dense on the curves. (Strictly speaking, the invariant sets are no longer continuous at the bifurcation point, but we will continue to refer to them as curves.) For quasiperiodically forced circle maps we can distinguish two types of these nonsmooth saddle-node bifurcations: one-sided and two-sided. In the one-sided nonsmooth saddle-node bifurcation, the collisions occur between pairs of invariant curves on the cylinder. An example is shown in Fig. 9(a) where the invariant curves and some of their translates by one in the x -direction are computed close to the bifurcation point. In the two-sided case each stable invariant curve on the cylinder touches both the unstable invariant curve immediately above it and the unstable invariant curve immediately below it. On the torus this implies that at the bifurcation point the attractor is everywhere discontinuous. An example of a two-sided nonsmooth saddle-node bifurcation is shown in Fig. 10(a). These two-sided nonsmooth saddle-node bifurcations are described in [Feudel et al., 1995], where it is shown that after the bifurcation (with $\Omega = 0$ and K fixed) the map has an SNA with unbounded motion in the x -direction (Fig. 10(b)) despite the fact that the rotation number remains zero due to the symmetry of Eqs. (2)–(3) when $\Omega = 0$. This implies that the diffusion in the x -direction is extremely slow; see [Feudel et al., 1995; Stark et al., 1999] for further details. In general, the two-sided nonsmooth saddle-node bifurcation is of codimension two, but it occurs as a codimension-1 phenomenon due to the symmetry if $\Omega = 0$. Figure 11 shows the range of dynamics observed in the third region of overlap in the plane $\Omega = 0$. Unbounded SNAs are observed in the blue regions and two-sided nonsmooth saddle-node bifurcations occur on the boundary between the white and blue regions.

The unbounded SNA of Fig. 10(b) must contain orbits which are unbounded above and orbits which are unbounded below [Stark et al., 1999]. This bidirectional diffusive motion of the unbounded SNA with $\Omega = 0$ becomes effectively unidirectional if $|\Omega|$ is very small, leading to a nonzero rotation number [Stark et al., 1999]. This suggests that these unbounded SNAs lie on the boundary of the phase-locked region. Fig. 12 shows this boundary in (ε, K, Ω) -space. It is clear that the height (i.e. the width in Ω) of the boundary is very small, if not zero, in regions of the (ε, K) plane with $\Omega = 0$ which have unbounded SNAs (compare the low plateau on the left of Fig. 12 with the region of unbounded SNAs of Fig. 11). As the height of the boundary becomes non-negligible we observe that the saddle-node bifurcation on the boundary has become one-sided (see Fig. 9), and we believe that it remains one-sided and nonsmooth throughout the red areas of Fig. 12 with non-negligible height. These red regions of the boundary correspond to saddle-node bifurcations with negative nontrivial Lyapunov exponents, and appear to precede the creation of SNAs with nonzero rotation numbers outside the phase-locked region [Ding et al., 1989; Glendinning, 1998].

If the phase-locked region really has zero height on the plateau, then it is wrong to refer to saddle-node bifurcations on the interior of the plateau: these points would correspond to a transition from an SNA with negative rotation number to an SNA with positive rotation number through an SNA with zero rotation number as Ω increases through zero. In this full three-parameter unfolding the two-sided nonsmooth saddle-node bifurcations are of codimension two, occurring on curves bounding the plateau and separating parts of the boundary of the phase-locked region with unbounded SNAs from parts with one-sided nonsmooth saddle-node bifurcations.

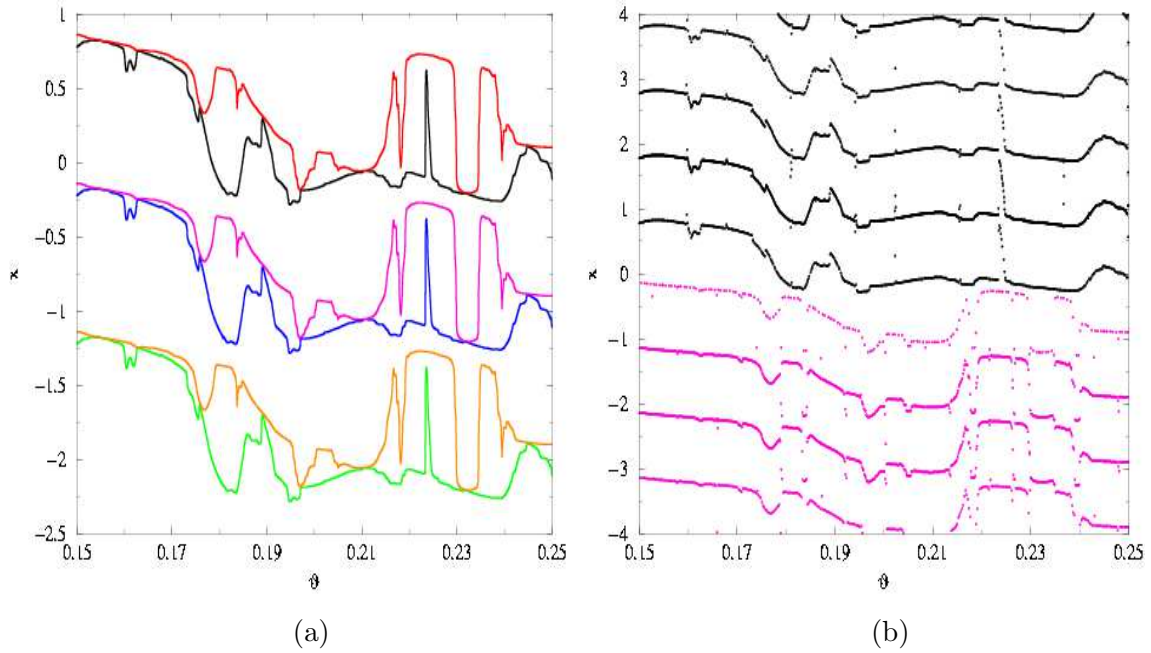


Figure 9: One-sided nonsmooth saddle-node bifurcation with $\Omega = 0.001$ and $\varepsilon = 2.58$: (a) before the collision ($K = 0.865$): attractors in black, blue and green, repellers in red, purple and orange; (b) after the collision ($K = 0.868$): attractor with the same initial condition as the black attracting invariant curve in (a); repeller with the same initial condition as the purple repelling invariant curve. The attractor moves upwards in forward time and the repeller moves downwards in reverse time. The rotation number is nonzero.

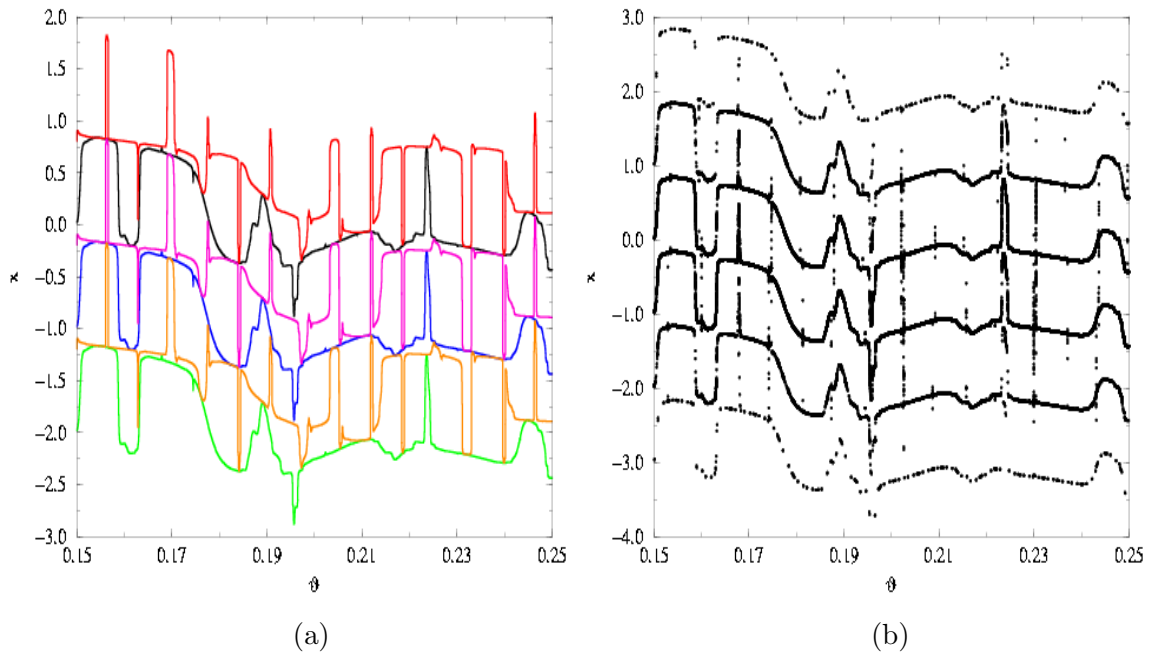


Figure 10: Two-sided nonsmooth saddle-node bifurcation with $\Omega = 0$ and $\varepsilon = 2.58$ (cf. the transition from the white to the blue region in Fig. 11): (a) before the collision ($K = 0.927$): attractors in black, blue and green, repellers in red, purple and orange; (b) after the collision ($K = 0.928$): SNA with the same initial condition as the black attracting invariant curve in (a). The strange repeller is not shown.

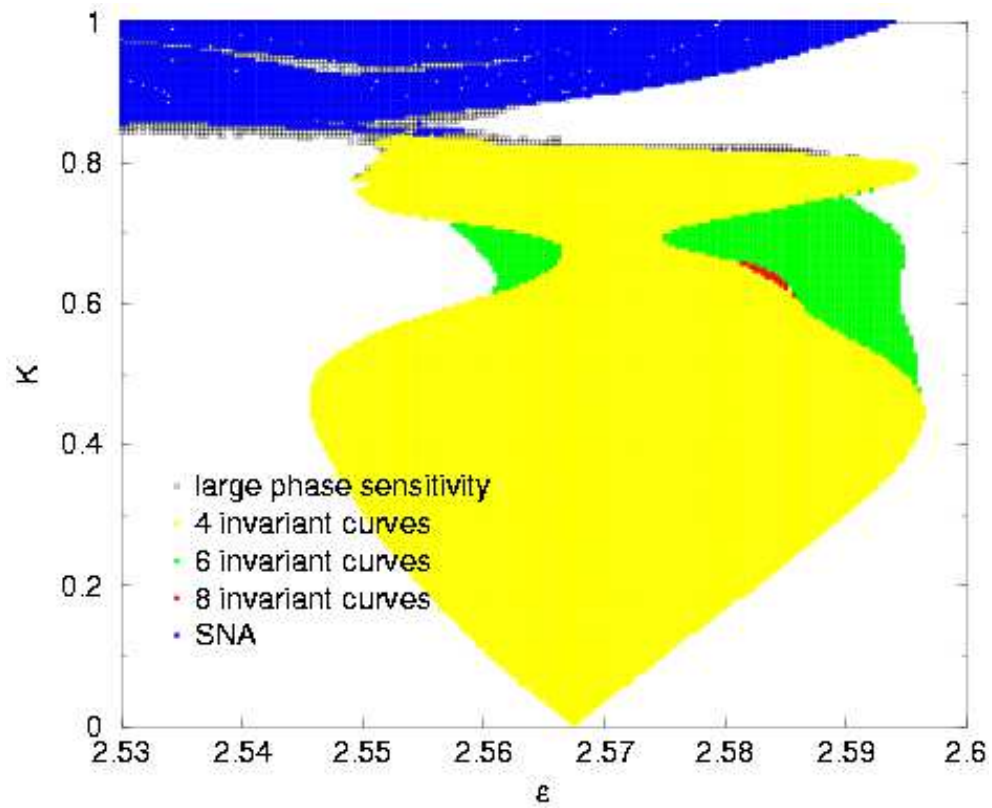


Figure 11: Section $\Omega = 0$ of the third overlap region. In the region of large phase sensitivity the attractor is very wrinkled or even an SNA.

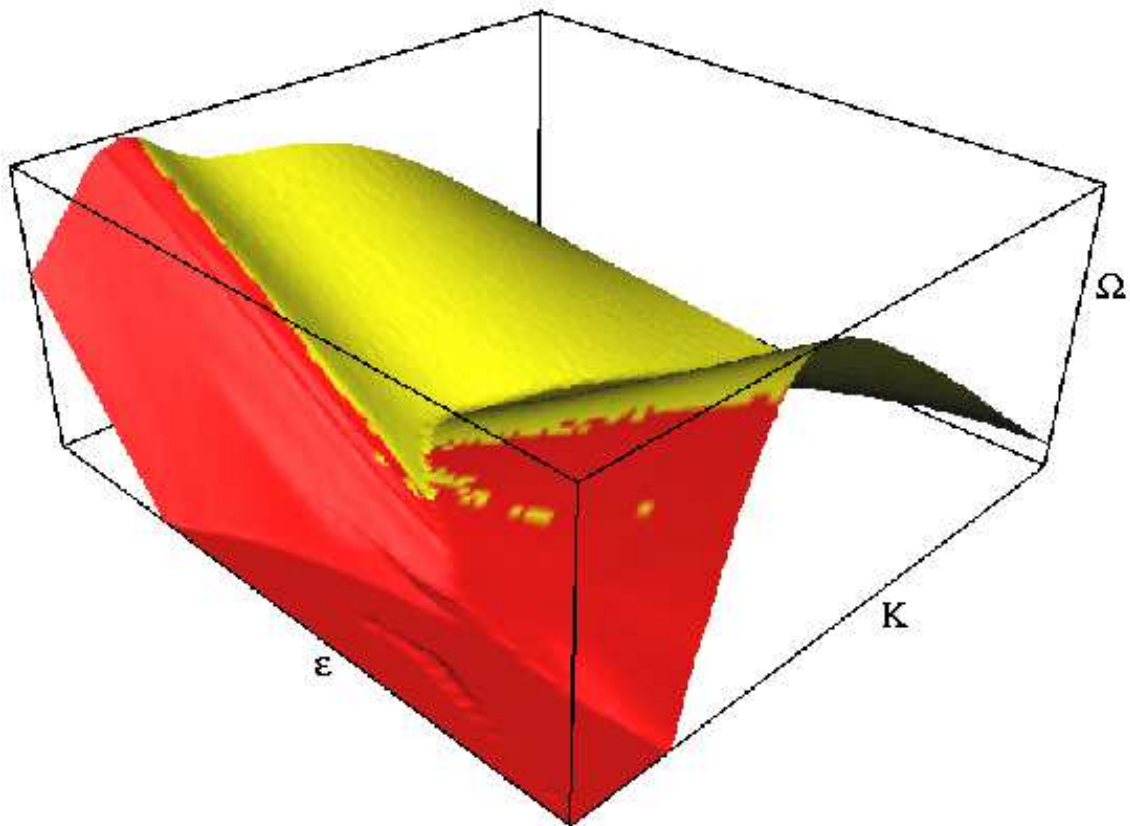


Figure 12: A small part of the boundary $|\Omega| = \Omega_0(\varepsilon, K)$ of the phase-locked region with zero rotation number; $\varepsilon \in [2.52, 2.62]$ runs from right to left, $K \in [0, 1]$ also from right to left, and $|\Omega| \in [0, 0.004]$ from bottom to top; compare Fig. 11. A grid of 80×160 points in the (ε, K) -plane is taken. Red regions with negative Lyapunov exponent (using $\lambda < -0.005$ as criterion) correspond to transitions to SNAs (the yellow spots are due to the finite threshold).

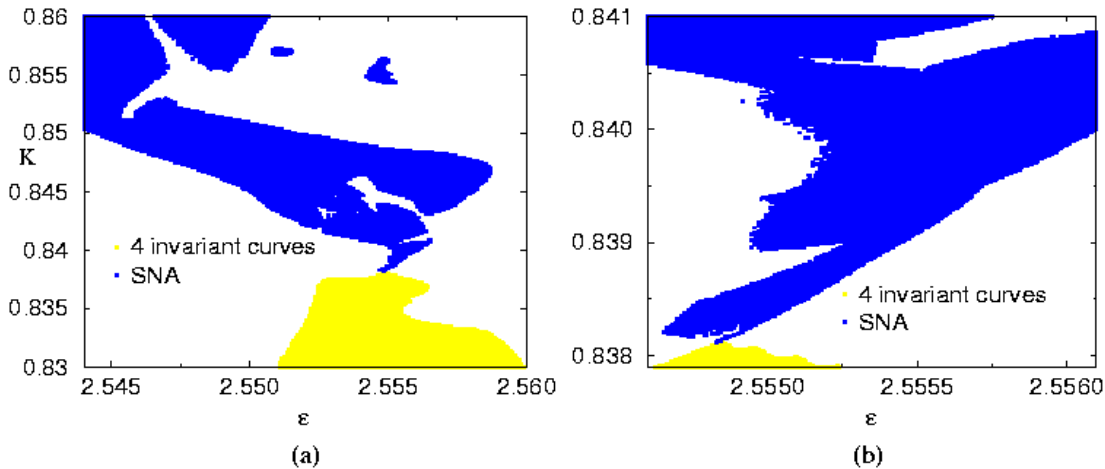


Figure 13: (a) Magnification of Fig. 11. The white region corresponds to pairs of invariant curves, regardless of their phase sensitivity. (b) Magnification of (a).

5 Nonsmooth bifurcation points of codimension two

In the full parameter space, and also already in the (ϵ, K) -plane with $\Omega = 0$, we expect codimension-2 bifurcations. We have already seen some of these; for example, the transition from yellow to red in Figs. 1 and 12 is the codimension-2 bifurcation curve marking the transition from a smooth saddle-node bifurcation to a nonsmooth one, respectively [Kuznetsov et al., 2000]. Another example is the codimension-2 point, mentioned in Sec. 4.2, where the smooth and nonsmooth pitchfork bifurcation curves meet. Note that there is no *curve* of codimension-2 points in this case, since the pitchfork bifurcation is restricted to the plane $\Omega = 0$. As discussed in the previous section, there is also the two-sided nonsmooth saddle-node bifurcation curve.

In this section we want to draw attention to an interesting codimension-2 point in the plane $\Omega = 0$. This point can be seen in Fig. 11 and in the enlargements Figs. 13(a)–(b) as the point where the region with unbounded SNAs (blue) and the bistable region (yellow) touch. It can be characterized as the moment where two nonsmooth (supercritical) pitchfork bifurcations happen simultaneously, i.e. a region of overlap is pulled apart; compare also the sketch in Fig. 7 of [Glendinning et al., 2000].

5.1 Smooth analog of the nonsmooth codimension-2 bifurcation point

Let us first discuss the smooth analog of this nonsmooth codimension-2 bifurcation point. Suppose for $\Omega = 0$ and some $K < 1$ fixed the bifurcation diagram involves only two supercritical pitchfork bifurcations that occur in the order as shown in Fig. 14(a). Now assume that as we increase K , this order is switched before we reach $K = 1$, without changing the type of pitchfork bifurcation from supercritical to subcritical. As shown in Fig. 14(b), this means that we necessarily need extra curves of saddle-node bifurcations.

The smooth analog of the nonsmooth codimension-2 bifurcation point is the point where the two pitchfork bifurcations happen at the same parameter values. In the (ϵ, K) -plane the complete bifurcation diagram should look like Fig. 15. The two supercritical pitchfork bifurcation curves are colored light-blue and magenta. The green and light-green curves are saddle-node bifurcation curves; compare also the colors in Figs. 14(a)–(b). Above the green and light-green curves, but below the light-blue and magenta curves there are four attractors. If we cross either

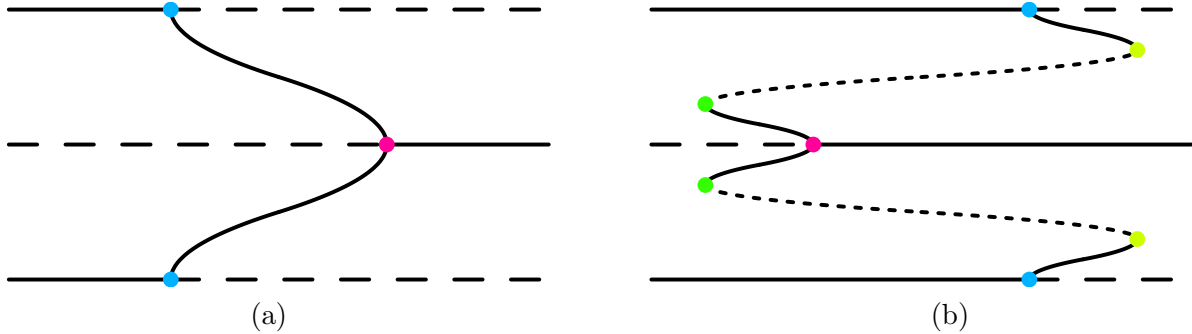


Figure 14: Two different bifurcation diagrams along the line $\Omega = 0$ that both involve two (smooth) supercritical pitchfork bifurcations. Shown are invariant curves (represented by one point) versus ε with K fixed. If the pitchfork bifurcation creating two attractors does not happen first, we necessarily need extra curves of saddle-node bifurcations (b).

the light-blue or the magenta curve from this region there are three attractors. Above the light-blue and magenta curves there are two attractors. We distinguish five qualitatively different K -intervals numbered I–V in Fig. 15. Interval I corresponds to Fig. 14(a) and V to Fig. 14(b). The qualitative behavior in the intervals II–IV is given in Figs. 16(a)–(c), respectively. The codimension-2 point that we are discussing here is the intersection point of the light-blue and magenta pitchfork bifurcation curves. The intersections of the green and light-blue curves, and the light-green and magenta curves are only intersections in this projection onto the (ε, K) -plane as can be seen in Fig. 16, where the transition from Fig. 16(a) to (b) marks the crossing of green and light-blue, and the transition from Fig. 16(b) to (c) represents the crossing of light-green and magenta.

5.2 A nonsmooth bifurcation point of codimension two

The nonsmooth version of Fig. 15 looks surprisingly simple in contrast; see Fig. 17. The coloring of the bifurcation curves is as in Fig. 15 with the restriction that all curves represent nonsmooth bifurcations. The upper pair of bifurcation curves corresponds to two-sided nonsmooth saddle-node bifurcations and the lower pair to nonsmooth pitchfork bifurcations.

We now have four regions with distinctive dynamics. To the left and to the right of the two pitchfork bifurcation curves there is one attractor. In between the two curves of pitchfork bifurcations there are two attractors. This is illustrated for a particular choice of the parameters in Fig. 18(b). The two attractors (black and blue) are two invariant curves separated by unstable invariant curves (green and red). In contrast to the previously discussed case of the nonsmooth pitchfork bifurcation, both unstable invariant curves are now close to the attracting invariant curves, because we are near the codimension-2 bifurcation point. The two different pitchfork bifurcations are illustrated in Figs. 18(a) and (c). If we decrease the forcing amplitude ε , the black, blue and green invariant curves disappear in a nonsmooth pitchfork bifurcation to form the green attractor coexisting with the red unstable invariant curve, as shown in Fig. 18(a). This corresponds to a crossing of the light-blue nonsmooth pitchfork bifurcation curve in Fig. 17. We cross the magenta nonsmooth pitchfork bifurcation curve in this figure by increasing ε . In this case the red, black and blue invariant curves disappear and form the red attractor coexisting with the green unstable invariant curve as in Fig. 18(c). The fourth region between the nonsmooth saddle-node bifurcations is characterized by the existence of unbounded SNAs.

Finally, we remark that the SNA region seems to have a fractal-like structure in the neighborhood of the codimension-2 point; compare Figs. 13(a)–(b). This would imply that the boundary

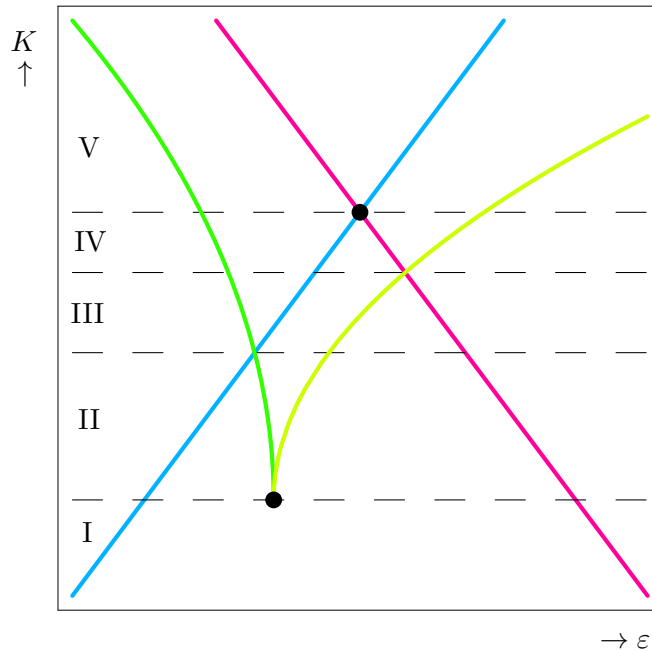


Figure 15: Unfolding of the smooth analog of the nonsmooth codimension-2 bifurcation point. Green and light-green curves are saddle-node bifurcations, light-blue and magenta curves correspond to pitchfork bifurcations.

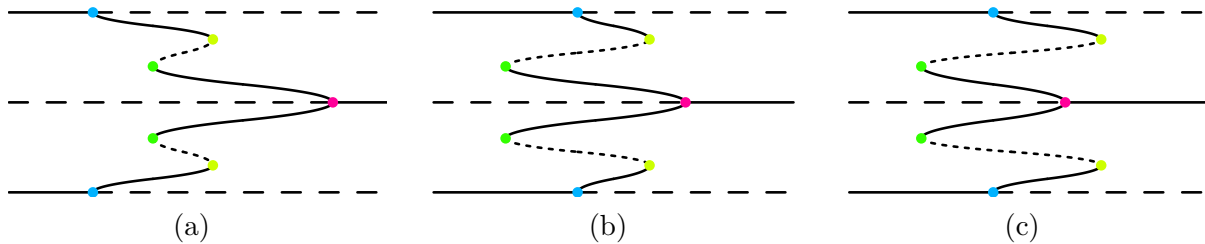


Figure 16: Qualitative bifurcation diagrams for K -values in the K -intervals II (a), III (b), and IV (c) in Fig. 15. The equivalent diagrams for the K -intervals I and V are shown in Fig. 14.

of the phase-locked region is fractal!

6 Tongues with Nonzero Rotation Numbers

We studied the structure of the phase-locked region with zero rotation number in great detail. In this section we briefly discuss the geometry of the tongues with nonzero rotation numbers that are close to the main tongue. More precisely, we determine the boundaries of the tongues with rotation numbers $\rho = 1/F_k$, with F_k the k th Fibonacci number $F_k = F_{k-1} + F_{k-2}$ and $F_1 = F_2 = 1$, using the same numerical procedure as before; see App. A.1. Several tongues for $K = 0.99$ are shown in Fig. 19. The fluctuations of the widths of the tongues with $\rho > 0$ are due to numerical errors, which are of the same magnitude as the widths themselves. The thick borderline $\Omega_0(\varepsilon, K)$ in this parameter regime corresponds to transitions to SNAs or bifurcations of SNAs of the type discussed in Sec. 4.3.

How these tongues approach the boundary $\Omega_0(\varepsilon, K)$ for fixed (ε, K) as k goes to infinity depends in general on ε and K ; compare $\varepsilon = 2.55$ and $\varepsilon = 2.61$ in Fig. 19. This behavior can be quantified with a scaling law for the distance $\Omega_\rho - \Omega_0$ between the main tongue and the tongues

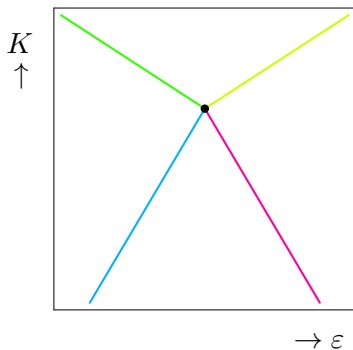


Figure 17: Unfolding of the nonsmooth codimension-2 bifurcation point. The green and light-green curves correspond to nonsmooth saddle-node bifurcations, while the light-blue and the magenta curves represent nonsmooth pitchfork bifurcations.

with nonzero rotation numbers ρ . We used several parameter pairs (ε, K) in Fig. 20 and our numerical calculations strongly suggest the scaling law $\rho \sim \Omega_\rho$ for ε and K such that $\Omega_0 = 0$, and $\rho \sim \sqrt{\Omega_\rho - \Omega_0}$ otherwise. This agrees with the linear scaling in the high- ε limit conjectured by Ding et al. [1989], the square-root scaling in the Arnol'd circle map for $\varepsilon = 0$ and $K > 0$ (see e.g. [MacKay & Tresser, 1984]) and the trivial linear scaling of the pure rotation for $\varepsilon = K = 0$. The square root scaling is associated with the one-sided saddle-node bifurcation, and the linear scaling is related to the change in the rotation number of the SNAs as in Sec. 4.3. The change between these scalings is associated with a two-sided nonsmooth saddle-node bifurcation point of codimension two at which two one-sided nonsmooth saddle-node bifurcation curves meet (presumably the nonsmooth analog of a cusp bifurcation point). A detailed study of this curve of codimension-2 points could be of interest.

7 Summary

We have studied the structure of the phase-locked regions in the quasiperiodically forced circle map. In particular, we have found regions of multistability where several attractors coexist. These regions of multistability appear due to the emergence of additional pairs of invariant curves as a result of saddle-node or pitchfork bifurcations under the variation of the forcing amplitude. As a result, these regions look like overlaps of phase-locked regions with the same rotation number.

Opening and closing of these pockets of multistability are due to saddle-node and pitchfork bifurcations of invariant curves. These bifurcations can be either smooth or nonsmooth depending on the strength of nonlinearity and the forcing amplitude. This is organized by the type of interaction between the stable and unstable invariant curves. In the smooth case these curves approach each other uniformly and then touch uniformly in each value of ϑ , so that the bifurcation looks like a simple merging of the invariant curves, analogous to the unforced case. Nonsmooth saddle-node bifurcations appear due to a wrinkled structure of the participating invariant curves, which collide at the bifurcation only in a dense set of ϑ -values. The result of this bifurcation is the emergence of a strange nonchaotic attractor. Similar to the nonsmooth saddle-node bifurcation we find a nonsmooth pitchfork bifurcation, but the details of this bifurcation are still unclear. Both for the saddle-node and the pitchfork bifurcation there are codimension-2 points in parameter space marking the transition from a smooth to a nonsmooth bifurcation. The exact determination of the codimension-2 pitchfork bifurcation point and the self-similarity properties in its neighborhood should be possible by using renormalization group

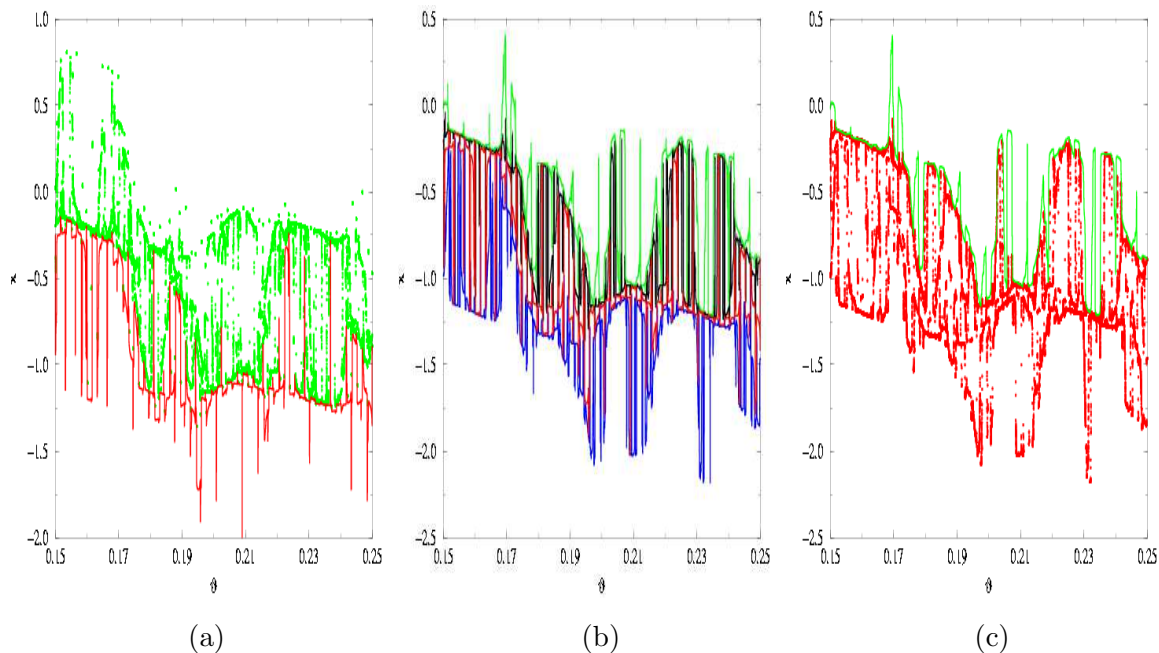


Figure 18: Nonsmooth pitchfork bifurcations in the neighborhood of the codimension-2 point $K = 0.83811$, $\Omega = 0$ and $\varepsilon = 2.55483$: (a) to the left of the bistable region ($K = 0.838$, $\varepsilon = 2.5542$); (b) within the bistable region close to the higher codimension point ($K = 0.838$, $\varepsilon = 2.55483$); (c) to the right of the bistable region ($K = 0.838$, $\varepsilon = 2.5551$).

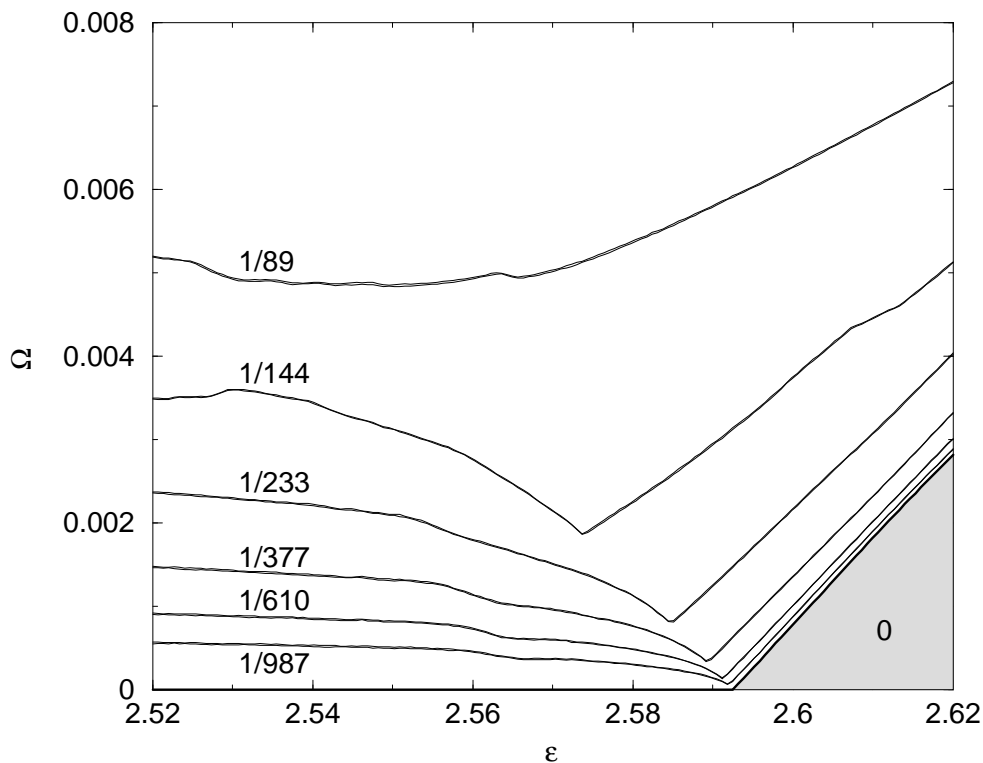


Figure 19: Section $K = 0.99$ of the regions with rotation numbers $\rho = 1/F_k$, k being $11, \dots, 16$, close to the (grey) region with $\rho = 0$; compare Figs. 11–12.

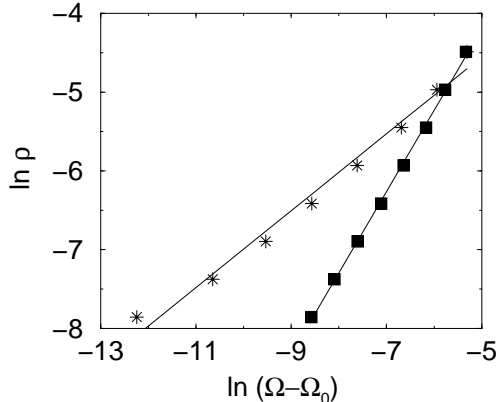


Figure 20: The distance $\Omega_\rho - \Omega_0$ of the tongue with rotation number $\rho = 1/F_k$ to the main tongue, where k ranges from 11 to 18; compare also Fig. 19. The data can be approximated by straight lines in a $\ln - \ln$ plot with slopes 1.032 ± 0.013 for $\varepsilon = 2.55$ (squares) and 0.488 ± 0.025 for $\varepsilon = 2.61$ (stars). The nonlinearity K is in both cases equal to 0.99.

techniques.

We have also investigated a nonsmooth codimension-2 bifurcation involving the merging of two nonsmooth pitchfork bifurcations and two nonsmooth saddle-node bifurcations which leads to regions of unbounded SNAs. This has no straightforward analog in smooth bifurcations.

The positions of phase-locked regions in the neighborhood of the region with zero rotation number were also described. Fixing the nonlinearity K and the forcing ε , we found that the rotation number ρ of these regions scales linearly with Ω_ρ whenever the width of the main tongue appears to be zero, and as $\sqrt{\Omega_\rho - \Omega_0}$ otherwise.

Acknowledgements

We thank for the hospitality of the Max Planck Institute for Physics of Complex Systems in Dresden, where this collaboration started during the Workshop and Seminar “Beyond Quasiperiodicity: Structures and Complex Dynamics” (January 1999), and where the work was completed in March 2000. H.O. was supported by an AFOSR/DDRE MURI grant AFS-5x-f496209610471 while she was employed at Caltech in Pasadena, USA. J.W. acknowledges financial support by the EU through a TMR Network on the dynamics of spatially extended systems under contract number FMRXCT960010. P.G. is grateful for a travel grant from the British Council. U.F. acknowledges financial support by the Deutsche Forschungsgemeinschaft (Heisenberg-Program and Sfb 555).

References

- Arnol’d, V. I. [1965] “Small denominators I,” *Trans. Amer. Math. Soc. 2nd. series* **46**, 213–284.
- Arnol’d, V. I. [1983] “Remarks on the perturbation-theory for problems of mathieu type,” *Russian Mathematical Surveys* **38**, 215–233.
- Bohr, T., Bak, P. & Jensen, M. H. [1984] “Transition to chaos by interaction of resonances in dissipative systems. II. Josephson junctions, charge-density waves, and standard maps,” *Phys. Rev. A* **30**, 1970–1981.
- Bohr, T., Bak, P. & Jensen, M. H. [1985] “Mode-locking and the transition to chaos in dissipative systems,” *Physica Scripta* **T9**, 50–58.

- Ding, M., Grebogi, C. & Ott, E. [1989] “Evolution of attractors in quasiperiodically forced systems: From quasiperiodic to strange nonchaotic to chaotic,” *Phys. Rev. A* **39**(5), 2593–2598.
- Feudel, U., Grebogi, C. & Ott, E. [1997] “Phase-locking in quasiperiodically forced systems,” *Physics Reports* **290**, 11–25.
- Feudel, U., Kurths, J. & Pikovsky, A. [1995] “Strange non-chaotic attractor in a quasiperiodically forced circle map,” *Physica* **88D**, 176–186.
- Glendinning, P. [1998] “Intermittency and strange nonchaotic attractors in quasiperiodically forced circle maps,” *Phys. Lett. A* **244**, 545–550.
- Glendinning, P., Feudel, U., Pikovsky, A. & Stark, J. [2000] “The structure of mode-locked regions in quasi-periodically forced circle maps,” (to appear in *Physica D*).
- Glendinning, P. & Wiersig, J. [1999] “Fine structure of mode-locked regions of the quasi-periodically forced circle map,” *Phys. Lett. A* **257**, 65–69.
- Grebogi, C., Ott, E., Pelikan, S. & Yorke, J. A. [1984] “Strange attractors that are not chaotic,” *Physica* **13D**, 261–268.
- Hall, G. R. [1984] “Resonance zones in two-parameter families of circle homeomorphisms,” *SIAM J. Math. Anal.* **15**(6), 1075–1081.
- Jensen, M. H., Bak, P. & Bohr, T. [1983] “Complete devil’s staircase, fractal dimension, and universality of mode-locking structure in the circle map,” *Phys. Rev. Lett.* **50**, 1637–1639.
- Jensen, M. H., Bak, P. & Bohr, T. [1984] “Transition to chaos by interaction of resonances in dissipative systems. I. circle maps,” *Phys. Rev. A* **30**, 1960–1969.
- Kuznetsov, S., Neumann, E., Pikovsky, A. & Sataev, I. [2000] “Critical point of tori-collision in quasiperiodically forced systems,” preprint, University of Potsdam (submitted to *Phys. Rev. E*).
- MacKay, R. S. & Tresser, C. [1984] “Transition to chaos for two-frequency systems,” *J. Physique Lett.* **45**, L741–L746.
- McGehee, R. P. & Peckham, B. B. [1996] “Arnold flames and resonance surface folds,” *Int. J. Bif. and Chaos* **6**, 315–336.
- Nishikawa, T. & Kaneko, K. [1996] “Fractalization of torus revisited as a strange nonchaotic attractor,” *Phys. Rev. E* **54**(6), 6114–6124.
- Osinga, H., Wiersig, J., Glendinning, P. & Feudel, U. [2000] “Multistability and non-smooth bifurcations in the quasiperiodically forced circle map,” <http://www.mpi-pks-dresden.mpg.de/eprint/jwiersig/0004003/>.
- Pikovsky, A. & Feudel, U. [1994] “Characterizing strange nonchaotic attractors,” *CHAOS* **5**(1), 253–260.
- Stark, J., Feudel, U., Glendinning, P. & Pikovsky, A. [1999] “Rotation numbers for quasiperiodically forced monotone circle maps,” preprint, University College London.
- Sturman, R. [1999] “Scaling of intermittent behaviour of a strange nonchaotic attractor,” *Phys. Lett. A* **259**, 355–365.

Appendix: Details on the Numerical Computations

We now explain our numerical computations in more detail and give values for the accuracy parameters. The Appendix is organized such that each section is related to one section in the main text. Appendix A.1 explains how to compute the tongue boundary for the main tongue with zero rotation number and relates to Sec. 2.2. Appendix A.2 discusses the generation of Fig. 6 in Sec. 4. Here, we also discuss how to identify SNAs using the phase sensitivity exponent, which is related to the derivative of x_n with respect to the external phase ϑ . The numerical issues that arise when determining the nonsmooth pitchfork bifurcation and the accompanying

fractalization process, as reported in Sec. 4.2, are described in more detail in App. A.3. In contrast to the method for identifying SNAs in the second region of overlap as described in App. A.2, we used another more efficient method for determining the regions where SNAs exist in the third region of overlap. This method is explained in App. A.4.

A.1 Numerical computation of the boundary of the phase-locked region

The boundary $\Omega = \Omega_0(\varepsilon, K)$ of the phase-locked region with $\rho = 0$ is half its width due to the symmetry. It is approximated by estimating the boundary point Ω_0 on a grid of 320×40 points in the (ε, K) -plane. Following [Stark et al., 1999] we determine the rotation number (4) within an accuracy of $\pm 1/N$ by averaging over a sample of 25 orbits of length $N = F_{28} = 317811$ (after 1000 preiterations to eliminate the effect of transients), where F_k are the Fibonacci numbers $F_1 = F_2 = 1$ and $F_k = F_{k-1} + F_{k-2}$. The Fibonacci numbers F_k are used since the value ϑ_{F_k} after F_k iterations is close to the initial value ϑ_0 due to the fact that ratios of Fibonacci numbers are good rational approximants of our irrational driving frequency ω . The initial interval $[\Omega_0^-, \Omega_0^+] = [0, 0.2]$ is repeatedly bisected, preserving the relation $\rho(\Omega_0^-) < 1/N < \rho(\Omega_0^+)$ to ensure that $\Omega_0 \in [\Omega_0^-, \Omega_0^+]$, until $\Omega_0^+ - \Omega_0^- < \Delta\Omega = 10^{-5}$. Finally, we choose Ω_0 to be the mean value of Ω_0^- and Ω_0^+ , or zero if the mean value is smaller than our numerical accuracy $\Delta\Omega$. Note that, as remarked in the Sec. 2.2, the question of whether Ω_0 really vanishes or is just very small cannot be answered by using only numerical methods.

To distinguish between smooth and nonsmooth saddle-node bifurcations of invariant curves on the boundary of the phase-locked region we compute the nontrivial Lyapunov exponent

$$\lambda(\Omega, \varepsilon, K) = \lim_{N \rightarrow \infty} \frac{1}{N} \sum_{n=0}^{N-1} \ln \left| \frac{\partial x_{n+1}}{\partial x_n} \right|_{(x_n, \vartheta_n)} = \lim_{N \rightarrow \infty} \frac{1}{N} \sum_{n=0}^{N-1} \ln |1 + K \cos 2\pi x_n|. \quad (5)$$

Vanishing λ (yellow regions in Fig. 1) indicates smooth saddle-node bifurcation while negative λ indicates nonsmooth saddle-node bifurcation (red regions); see Feudel et al. [1997] and Sec. 2.2.

A.2 The cross-section $\Omega = 0$ of the second region of overlap

Figure 6 shows the bifurcation structure at a cross-section $\Omega = 0$. The picture was generated as follows. For each grid point $N = F_{32} = 2178309$ iterations of Eqs. (2)–(3) were computed using 25 different initial conditions $(x_0, \vartheta_0 = 0)$. We take advantage of the fact that inside the tongue with zero rotation number, each attractor is represented as a single-valued function $x = X(\vartheta)$, $\vartheta \in [0, 1)$. (This function is smooth in the case of a nonstrange attractor and discontinuous everywhere in the case of an SNA.) This means that the number of different attractors is equal to the number of different N th iterates, i.e., different x_N -values. By setting a tolerance of $\pm 10^{-6}$ the number of attractors was determined numerically.

To identify the emergence of SNAs, we compute the attractors and quantify their smoothness properties using the so-called phase sensitivity exponent introduced by Pikovsky and Feudel [1994]. By formally differentiating Eq. (2) with respect to the external phase ϑ , we get

$$\frac{\partial x_{n+1}}{\partial \vartheta} = (1 + K \cos 2\pi x_n) \frac{\partial x_n}{\partial \vartheta} + 2\pi \varepsilon \cos 2\pi \vartheta_n. \quad (6)$$

When Eq. (6) is iterated together with Eqs. (2)–(3), starting from some initial point (x_0, ϑ_0) and $\partial x_0 / \partial \vartheta = 0$, the phase sensitivity

$$\Gamma_N = \min_{(x_0, \vartheta_0)} \max_{0 \leq n \leq N} \left| \frac{\partial x_n}{\partial \vartheta} \right| \quad (7)$$

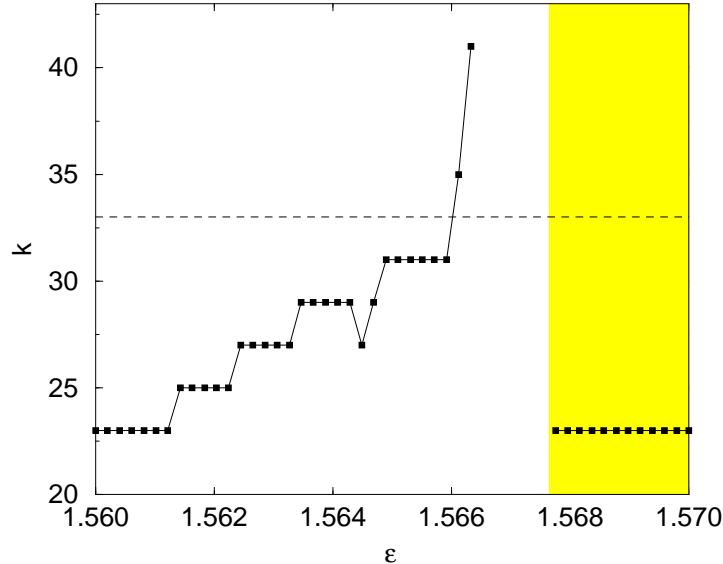


Figure 21: Minimum number of iterations F_k for which the phase sensitivity saturates, as a function of ε , with $K = 0.9$ and $\Omega = 0$. Compare with Fig. 6, where $k = 33$ (dashed line) is used as a threshold. In the yellow marked interval the phase sensitivity always saturates for $k = 23$, indicating two smooth attracting invariant curves. In the white marked interval with ε smaller than ≈ 1.566 saturations occurs for $k \leq 41$, indicating a quite wrinkled but smooth attracting invariant curve. Using a maximum of F_{43} iterations, there is no saturation for larger ε .

diverges like N^μ for large N in the case of an SNA. On the other hand, in the case of a smooth attractor it saturates, i.e. the phase sensitivity exponent μ is zero. The criteria for saturation we employ are $\Gamma_N < 10^{15}$ and $\mu < 0.25$ (obtained by fitting the slope in a ln-ln diagram using three different N s). The black area in Fig. 6 shows the parameter region for which Γ_N does not saturate when eight different initial points are iterated for up to $N = F_{33} = 3\,524\,578$ time steps. How much of this black area persists as N tends to infinity? Figure 21 provides more numerical results for larger N and fixed $K = 0.9$, showing the minimum number of iterations $N = F_k$ (in terms of the index of the Fibonacci number) for which the phase sensitivity saturates versus the forcing amplitude ε . Although a large number of iterations, $F_{43} = 433\,494\,437$, was used, saturation occurs only for $\varepsilon \leq 1.566$ and $\varepsilon \geq 1.568$. Hence the interval $\varepsilon \in [1.566, 1.568]$ contains the nonsmooth pitchfork bifurcation point, as described in Sec. 4.2, which is approximately 1.5676. In the next section we discuss the numerical determination of the length of this gap.

A.3 Numerical issues regarding the nonsmooth pitchfork bifurcation

Figure 21 shows the minimum number of iterations $N = F_k$ (in terms of the index of the Fibonacci number) for which the phase sensitivity exponent converges, versus ε . There is no convergence of the phase sensitivity exponent, even for N as large as $F_{43} = 433\,494\,437$, in the interval $\varepsilon \in [1.566, 1.568]$. Close to the right side of this interval, a pitchfork bifurcation occurs, because there is one smooth attractor (white region in Fig. 21) for smaller ε and there are two smooth attractors (yellow region) for larger ε . Hence, we clearly have a gap when we bound the number of iterations by $F_k = F_{43}$, but it is unclear whether this gap has nonzero width as $k \rightarrow \infty$.

There are other methods to assess the smoothness properties of the attractor(s). For example, in Fig. 22 we applied the method of rational approximations. This method is based on the approximation of the irrational frequency ω by rational frequencies $\omega_k = F_{k-1}/F_k$ with $k \in \mathbb{N}$ and $\omega = \lim_{k \rightarrow \infty} \omega_k$, replacing the quasiperiodically forced map (2)–(3) with a sequence of

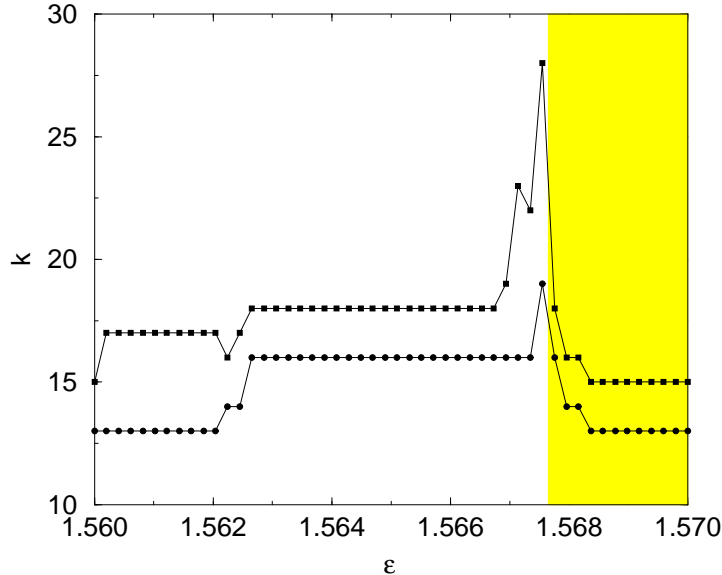


Figure 22: Minimum order k of the rational approximation for which the sensitive dependence on the initial phase ϑ_0 vanishes (lower curve) and for which the maximum derivative of the attracting sets in $\vartheta_0 \in [0, 1)$ saturates (upper curve), as a function of ε with $K = 0.9$ and $\Omega = 0$, cf. Fig. 21. We used 1000 different values of $\vartheta_0 \in [0, 1/F_k)$.

periodically (with period F_k) forced maps. The F_k th iteration of such a map is an orientation-preserving diffeomorphism on a circle depending on (Ω, ε, K) and on the initial phase ϑ_0 . The union of all attracting invariant sets of this family of diffeomorphisms with $\vartheta_0 \in [0, 1/F_k)$, forms the k th approximation of the attractors of the quasiperiodically forced system. (It is sufficient to consider the subinterval $[0, 1/F_k)$, since diffeomorphisms with $\vartheta_0 \in [n/F_k, (n+1)/F_k)$, $n = 1, 2, \dots, F_k - 1$, are topologically conjugate.) For smooth attractors there is a number k for which the rational approximation of order k and larger does not depend sensitively on ϑ_0 [Pikovsky & Feudel, 1994].

Figure 22 shows that this is here the case: the dependence on the initial phase for moderate k — one or two stable fixed points for all ε , depending on ϑ_0 — disappears as we cross the lower curve towards higher k values — one stable fixed point in the white marked interval, corresponding to a single smooth attractor in the quasiperiodically forced map, and two stable fixed points in the yellow marked interval, corresponding to a pair of smooth attractors.

However, as mentioned in [Pikovsky & Feudel, 1994], a vanishing dependence on ϑ_0 is a necessary but not sufficient condition for smoothness. We also have to stipulate that the maximum derivative of the attracting sets with respect to ϑ_0 is bounded for all $\vartheta_0 \in [0, 1)$ as $k \rightarrow \infty$. Note that it is nevertheless sufficient to determine the attracting sets only in the subinterval $[0, 1/F_k)$ since the other parts can be obtained by iterating the map (2)–(3) with the rational frequency ω_k . Furthermore, it is elegant to iterate Eq. (6) simultaneously in order to determine the derivative. The maximum derivative obtained by this procedure is an approximation of the phase sensitivity. Using the same criteria for boundedness as before, we surprisingly find that the maximum derivative always saturates at some order k , shown by the upper curve in Fig. 22. The qualitative features of Figs. 21–22 persist if we choose different K 's in the region with large phase sensitivity.

A.4 SNAs in the third region of overlap

To compute SNAs near the boundary of the tongue in the third region of overlap we use a more effective method than the method described in App. A.2. This method takes advantage of the fact that the corresponding SNAs are unbounded in the x -direction in the lift of the map. We define the amplitude of an attractor at time N as

$$\tilde{\Gamma}_N = \min_{(x_0, \vartheta_0)} \left(\max_{0 \leq n \leq N} x_n - \min_{0 \leq n \leq N} x_n \right).$$

For an unbounded SNA the asymptotic behavior of the amplitude is given by $c \ln N$ [Feudel et al., 1995], in all other cases the amplitude saturates for large N . The numerical algorithm is almost the same as for the phase sensitivity (7). However, by fitting the slope using four different N , we find as criteria for saturation $\tilde{\Gamma}_N < 6.0$ and $c < 0.02$. Therefore, typically far less iterations are necessary, so that a larger maximum number of iterations $N = F_{40} = 102\,334\,155$ and 10 different initial conditions can be used.